Quantum Storage of Photonic Entanglement in a Crystal

Christoph Clausen,* Imam Usmani,* Félix Bussières, Nicolas Sangouard,
Mikael Afzelius, Hugues de Riedmatten, and Nicolas Gisin
Group of Applied Physics, University of Geneva, CH-1211 Geneva 4, Switzerland
(Dated: November 12, 2010)

arXiv:1009.0489v3 [quant-ph] 10 Nov 2010

Entanglement is the fundamental characteristic of quantum physics. Large experimental efforts are devoted to harness entanglement between various physical systems. In particular, entanglement between light and material systems is interesting due to their prospective roles as "flying" and stationary qubits in future quantum information technologies, such as quantum repeaters [1–3] and quantum networks [4]. Here we report the first demonstration of entanglement between a photon at telecommunication wavelength and a single collective atomic excitation stored in a crystal. One photon from an energy-time entangled pair [5] is mapped onto a crystal and then released into a well-defined spatial mode after a predetermined storage time. The other photon is at telecommunication wavelength and is sent directly through a 50 m fiber link to an analyzer. Successful transfer of entanglement to the crystal and back is proven by a violation of the Clauser-Horne-Shimony-Holt (CHSH) inequality [6] by almost three standard deviations ($S = 2.64 \pm 0.23$). These results represent an important step towards quantum communication technologies based on solid-state devices. In particular, our resources pave the way for building efficient multiplexed quantum repeaters [7, 8] for long-distance quantum networks.

While single atoms [9, 10] and cold atomic gases [11–16] are currently some of the most advanced light-matter quantum interfaces, there is a strong motivation to control light-matter entanglement with more practical systems, such as solid-state devices [17]. Solid-state quantum memories for photons can be implemented with cryogenically cooled crystals doped with rare-earth-metal (RE) ions [18], which have impressive coherence properties at temperatures below 4 K. These solid-state systems have the advantage of simple implementation since RE-doped crystals are widely produced for solid-state lasers, and closed-cycle cryogenic coolers are commercially available. Important progress has been made over the last years in the context of light storage into solid-state memories, including long storage times [19], high efficiency [20] and storage of light at the single photon level with high coherence and negligible noise [8, 20–24]. Yet, these experiments were realized with classical bright or weak coherent states of light. While this is sufficient to characterize the performances of the memory, and even to infer the quantum characteristics of the device [20, 21], it is not sufficient for the implementation of more sophisticated experiments involving entanglement, as required for most applications in quantum information science. For this purpose, it is necessary to store non-classical light, in particular individual photons that are part of an entangled state. In addition, for quantum communication applications, the other part of the entangled state should be a photon at telecommunication wavelength in order to minimize loss during transmission in optical fibers.

In this Letter, we report on an experiment where a photon from an entangled pair is stored in a quantum memory based on a RE-doped crystal. The quantum properties of the photon persist after the retrieval from the memory. More specifically, we show that the non-classical nature of the intensity correlations is preserved, and that the entanglement fidelity of the retrieved photon is sufficient to violate a Bell inequality. Such a violation is explicitly demonstrated. These results represent the first successful demonstration of the reversible mapping of energy time entangled photons onto and out of a quantum memory.

EXPERIMENT

Our experiment consists of a coherent solid-state quantum memory and a source of entangled photons. The complete experimental setup, comprising the source of entangled photon pairs and quantum memory, is shown in Fig. 1.

The source is based on non-degenerate spontaneous parametric down conversion (SPDC) in a non-linear PPKTP waveguide pumped by continuous wave light at 532 nm, yielding energy-time entangled photons with the signal photon at the memory wavelength of 883 nm, and the idler photon at the telecom wavelength of 1338 nm. Both photons initially have a spectral width of approximately 1.5 THz, a factor of 10^4 larger than the 120 MHz bandwidth of the memory. Hence, strong filtering is crucial [25] to achieve signal-to-noise ratios sufficiently large to reveal the presence of entanglement after the storage (see Fig. 1 and Supplementary Information). Additionally, active frequency stabilization was necessary to maintain the simultaneous spectral overlap of the photon pairs with the filtering system and the quantum memory (see Supplementary Information).

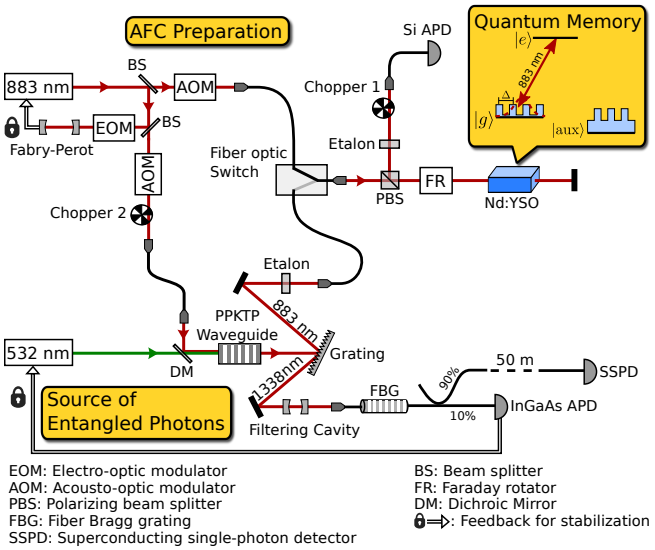

FIG. 1. **Experimental setup**. The experimental setup can be divided into three parts: The crystal serving as quantum memory, the laser system for the preparation of the atomic frequency comb (AFC) in the crystal, and the source of entangled photons with associated spectral filtering. During the experiment we periodically switch between 15 ms of AFC preparation followed by a 15 ms measurement phase, where entangled photons are stored. During the preparation, the comb structure is prepared by frequency-selective optical pumping using light from an 883 nm diode laser in combination with an acousto-optic modulator. The fiber optic switch is in the upper position, and the silicon avalanche photodiode (Si APD) is protected from the bright light by chopper 1. At the same time, we must ensure that the central frequency of the optical filtering system at 1338 nm and of the AFC at 883 nm both satisfy the energy conservation of the SPDC process. To this end, chopper 2 is opened, and a small fraction of the light at 883 nm is overlapped with the light of the 532 nm continuous wave laser that pumps the PPKTP waveguide. This leads to the creation of light at 1338 nm by difference frequency generation (DFG). Using this DFG signal, the frequency of the 532 nm light is adjusted such the detection rate on a separate InGaAs APD stays constant, which means that the 1338 nm DFG light is in resonance with the filtering cavity. Long-term stability of the 883 nm laser itself is achieved by continuously referencing it to a Fabry-Perot cavity. During the measurement phase, the positions of switch and choppers are reversed. Now, entangled pairs of photons are generated in the waveguide via SPDC. The two photons in a pair are spatially separated by a diffraction grating and then strongly filtered. The filtering at 1338 nm consists of a cavity followed by a fiber Bragg grating that removes spurious longitudinal modes of the cavity. Then the photons are directed towards a superconducting single photon detector located in another laboratory 50 m away. The photons at 883 nm undergo filtering by two etalons with different free spectral ranges, such that only photons within a narrow range of frequencies pass through both etalons. The photons are sent through the crystal in a double-pass configuration to increase the absorption probability, and are afterwards detected by the Si APD. See Supplementary Information for more details.

The quantum memory is a Y_2SiO_5 crystal impurity-doped with neodymium ions having a resonance at 883 nm with good coherence properties [8]. It is based on a photon echo type interaction using an atomic frequency comb (AFC) [26]. In an AFC the absorption profile of the atomic ensemble is shaped into a comb-like structure by optical pumping. A photon is then, with some efficiency, absorbed and re-emitted into a well-defined spatial mode due to a collective rephasing of the atoms in the comb structure. The time of re-emission depends on the period of the comb and is pre-determined. Using weak coherent states, we have previously shown that our memory is capable of coherently storing multiple temporal modes [8]. Therefore, this type of interface is perfectly suited for storing true single photons created at random times, as is the case for energy-time entanglement. Nevertheless, switching to photons generated by SPDC posed major challenges. Besides the elaborate filtering of the photons and its associated frequency stabilization, it was necessary to significantly increase the storage efficiency. Employing a new optical pumping scheme for the preparation of the AFC (see Supplementary Information), the efficiency was increased by a factor of 3 for storage times below 200 ns, now reaching values up to 21% (see results below). After being released from the memory, the photon at 883 nm is detected with a single-photon avalanche photodiode. The filtered photon at 1338 nm is sent to another laboratory 50 m away via a single mode fiber, where it is analyzed and detected using a superconducting single photon detector (SSPD). Owing to the low loss at telecommunication wavelengths, the amount of optical fiber could in principle be extended to several kilometres without significantly affecting the results presented herein.

RESULTS

Non-classical correlations

In a first experiment we verified that the non-classical nature of the intensity correlations between the two photons is preserved during the storage and retrieval process. Neglecting the exact frequency dependence, the state of the photons created in the SPDC process, provided that the pair creation probability p is much smaller than 1, is described by

$$|0_s, 0_i\rangle + \sqrt{p}|1_s, 1_i\rangle + O(p), \qquad (1)$$

where the subscript s (i) indicates the signal (idler) mode at 883 nm (1338 nm). While in such a state both the signal and idler modes individually exhibit the statistics of a classical thermal field, its quantum nature can be revealed by strong intensity correlations between the two modes. Indeed, assuming second-order auto-correlations

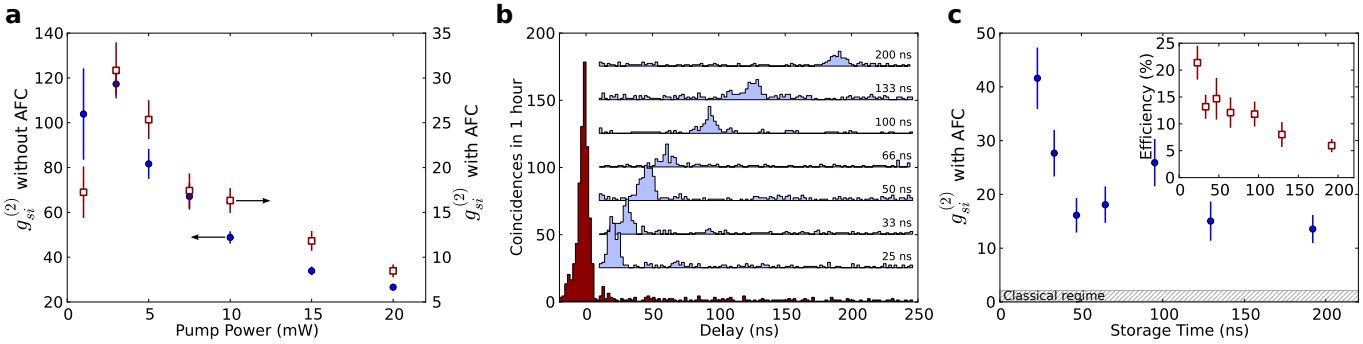

FIG. 2. **Measurements of the cross-correlation and storage efficiency**. (a) Cross-correlation $g_{si}^{(2)}$ as a function of the pump power. Data points shown were taken with an AFC memory storage time of 25 ns (empty squares), and for comparison, with the crystal prepared with a 120 MHz wide transmission window, i.e. without AFC (filled circles). We achieve the highest correlations for a pump power around 3 mW. The size of the coincidence window is 10 ns. (b) Coincidence histograms for different storage times. Individual histograms are vertically offset for clarity. Each histogram shows a peak at the pre-determined storage time. For comparison, the bottom-most histogram (red) was taken without AFC. (c) Cross-correlation $g_{si}^{(2)}$ as a function of storage time with 10 ns coincidence window, extracted from (b). For storage times up to 200 ns the correlations stay well above the classical regime given by Eq. (2) (shaded area). The inset shows the storage efficiency for the same range of storage times.

of signal and idler of $g_s^{(2)} = g_i^{(2)} = 2$, a lower bound of the cross-correlation function $g_{si}^{(2)}$ gives a criterion for non-classicality [27],

$$g_{si}^{(2)} = \frac{P_{si}}{P_s P_i} > \frac{1}{2}\left(g_s^{(2)} + g_i^{(2)}\right) = 2, \qquad (2)$$

where P_s (P_i) is the probability to detect a signal (idler) photon, and P_{si} the probability for a coincidence detection. In practice, P_{si} ($P_s P_i$) is determined by the number of coincidences in a certain time window centered on (away from) the coincidence peak.

To find the optimum conditions for the experiment, we first measured the cross-correlation as a function of the pump power of the source, as shown in Fig. 2a. In one measurement series we used an AFC with 25 ns storage time. For comparison, we took a second series with the crystal prepared without the AFC, that is, with a 120 MHz wide transmission window. In both cases, the results are typical for photons from an SPDC source. For low pump powers, the cross-correlation is limited by detector dark counts, and at high pump powers it is reduced by the contribution of multiple pairs, i.e. the higher order terms in (1). We find an optimum around a pump power of 3 mW, where $g_{si}^{(2)} \simeq 115$ without AFC, and $g_{si}^{(2)} \simeq 30$ after a 25 ns storage, thus proving the quantum character of the storage. The reduction in the cross-correlation with the storage is due to limited efficiency (21%). This can be considered as loss which effectively increases the contribution of accidental coincidences stemming from dark counts and multiple pair emissions.

Next, we measured the memory efficiency and the cross-correlation for different storage times, as shown in Fig. 2b and 2c. The efficiency is defined as the ratio of the number of stored and released photons to the total number of photons incident on the crystal, and includes effects of decoherence in the memory [8]. The longer the storage time, the more difficult it is to prepare a comb with optimal shape (see Supplementary Information). This is due to material limitations and leads to a decrease of efficiency, and consequently to a decrease of the cross-correlation. However, the latter stays well above the classical limit for storage times up to 200 ns. Possibilities to extend this storage time will be discussed below.

Entanglement

We now turn our attention towards the most particular kind of quantum correlations, namely entanglement. By performing a two-photon quantum interference experiment, we show that the entanglement of the photon pair is preserved when the signal photon is stored in the crystal.

Photon pairs generated by our source are energy-time entangled, that is, the two photons in a pair are created simultaneously to ensure energy conservation, but the pair creation time is uncertain to within the coherence time of the pump laser. We want to reveal the presence of this entanglement using a Franson-type setup [5], see Fig. 3a. Such a setup requires two equally unbalanced interferometers with delay τ larger than the coherence time of the photons (here about 5 ns), so there can be no single-photon interference. If additionally the delay is shorter than the coherence time of the pump, the uncertainty in the creation time will lead to quantum interference between the two path combinations short-short

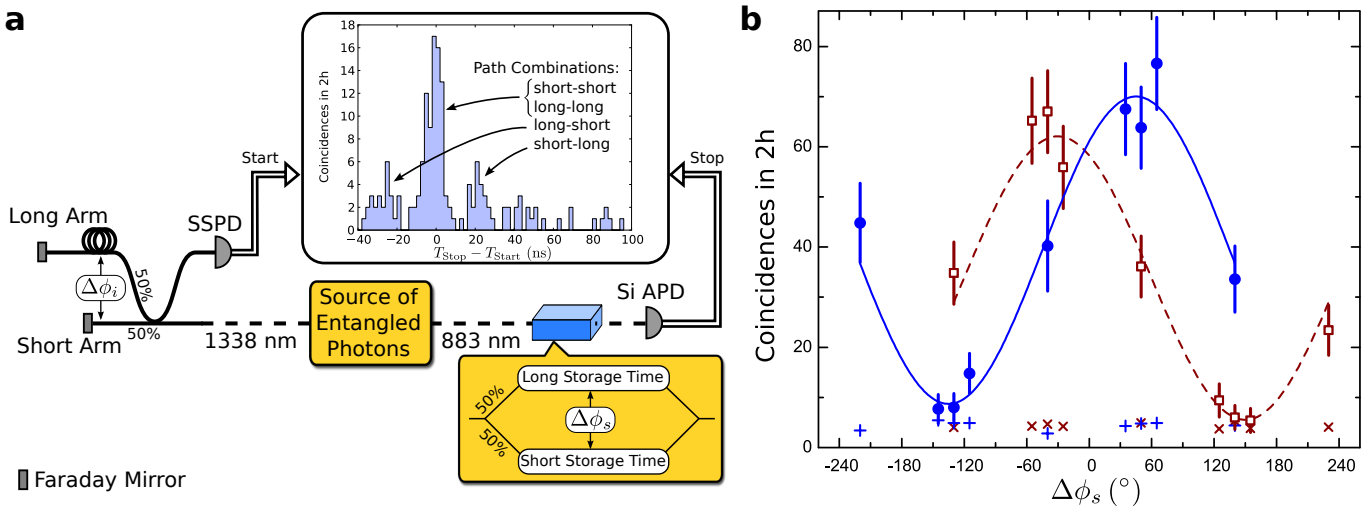

FIG. 3. **Entanglement preservation during the quantum storage**. (a) To reveal the presence of energy-time entanglement, we used a Franson-type setup. A fiber interferometer with $\tau = 25$ ns path length difference was inserted before the detector of the idler photon. For the signal photon, the interferometer was implemented using the quantum memory with partial read-outs with a short storage time of 50 ns and a long storage time of 75 ns. The resulting coincidence histogram shows three peaks separated by τ corresponding to different path combinations. Due to interference, the coincidence probability at zero time-delay, i.e. in the central peak, oscillates as a function of both of the relative phases $\Delta\phi_s$ and $\Delta\phi_i$, given by Eq. (3). (b) Number of coincidences in the central peak in two hours as a function of the relative phase $\Delta\phi_s$ for two values of $\Delta\phi_i$. The pump power was 5 mW, and the size of the coincidence window 10 ns. The solid and dashed lines result from fits to Eq. (3) and respectively give visibilities of $V = 78 \pm 4\%$ and $84 \pm 4\%$. The visibilities are mainly limited by the level of accidental coincidences (crosses). The fit also gives a difference between the two values of $\Delta\phi_i$ of $75 \pm 10°$. These values closely match settings necessary for a maximal violation of the CHSH inequality.

and long-long. The interference manifests itself in the coincidence probability [5],

$$P_{si} \propto 1 + V\cos(\Delta\phi_s + \Delta\phi_i), \tag{3}$$

where V is the visibility of interference, and $\Delta\phi_{s,i}$ are the relative phases acquired between the short and long arms in the signal and idler interferometers, respectively. The observed interference can also be interpreted as a post-selection of a time-bin entangled state,

$$\frac{1}{\sqrt{2}}\left(|E_s E_i\rangle + |L_s L_i\rangle\right), \tag{4}$$

with a time difference $\tau = 25$ ns between the early (E) and late (L) time-bins. For the idler photon we used a fiber interferometer, while for the signal photon, we implemented the interferometer by the technique of partial read-outs [21] of the AFC at two storage times separated by τ, which gives us excellent control over $\Delta\phi_s$. Note that the temporal multi-mode capability [8, 26, 28] is necessary to coherently map the signal time-bin qubit onto a collective atomic excitation upon absorption.

Figure 3b shows the measured coincidence rate as a function of $\Delta\phi_s$ for two values of $\Delta\phi_i$ and a source pump power of 5 mW. The visibility of the interference is $V = 84 \pm 4\%$ and $78 \pm 4\%$, which corresponds to a mean two-qubit fidelity with the input state of $F = 86 \pm 2\%$. Hence, according to the Peres criterion [29] of $F \geq 0.5$, the two photons are still entangled after the quantum storage. This also means that while the signal photon was still inside the crystal, the post-selected entangled state (neglecting noise) was of the form

$$\frac{1}{\sqrt{2}}\left(|E_{QM} E_i\rangle + |L_{QM} L_i\rangle\right), \tag{5}$$

that is, the idler photon was entangled with a collective atomic excitation inside the quantum memory, denoted by the subscript QM.

The nonlocal character of the entanglement can be revealed by a violation of the Clauser-Horne-Shimony-Holt (CHSH) inequality [6]. Note that the possibility to violate this inequality can be inferred indirectly from a visibility larger than 71%. Nevertheless, we performed the measurements necessary for a direct violation of the inequality and obtained $S = 2.64 \pm 0.23$ (details are given in the Supplementary Information). This proves the presence of nonlocal quantum correlations between the telecom photon and a collective atomic excitation in the crystal, and hence the presence of entanglement independent of the experimental details [30]. At the same time, this would guarantee the security against individual attacks for quantum key distribution applications [30].

Bell test involving hybrid qubit

A particularly intriguing situation arises when instead of using two modes of the partial read-out as a time-bin qubit, one uses a single read-out together with the transmitted part of the photon as time-bins. Indeed, the imbalance between the storage efficiency and the transmission probability offers a well suited qubit analyzer for a violation of the CHSH inequality using bases lying in the xz-plane of the Bloch sphere [31] (see Supplementary Information). We performed such a measurement and observed $S = 2.62 \pm 0.15$, i.e. a violation by more than 4 standard deviations. This is an entanglement witness showing that at any step before the detections, the initial entanglement (4) was preserved. In particular, this implies that while the early mode was stored in the crystal, the two-qubit state (neglecting noise and omitting normalisation) was of the form

$$\alpha|E_{QM}E_i\rangle + |L_sL_i\rangle, \tag{6}$$

where α is related to the absorption efficiency η_{abs} of the quantum memory by $\alpha = \sqrt{\eta_{\text{abs}}}$. This is an entangled state between a telecommunication-wavelength qubit and a photon-crystal hybrid qubit. We note that this kind of hybrid qubit is the key ingredient of one of the most efficient quantum repeaters based on atomic ensembles and linear optics [32].

OUTLOOK

The fact that one can create entanglement between a single photon and a macroscopic object – in this case a collective atomic excitation delocalized over a 1 cm long crystal – is fascinating in itself. Beyond their fundamental interest, the results presented in this Letter are part of the effort towards the long-term goal of the implementation of an efficient quantum repeater. Quantum repeaters are a promising solution to the problem of finite loss in optical fibers, which at the moment limits the practical distance for entanglement distribution and quantum cryptography [3]. Our results show that commercial crystals can be used as quantum memory for entangled photons. This represents an important enabling step towards solid state based quantum repeaters. The next major challenges are clearly identified: longer storage times, the possibility for on-demand read-out of the memory and higher efficiency. Promising ideas and encouraging results in these individual directions do already exist. Crystals of Y_2SiO_5 doped with praseodymium or europium have a suitable energy-level structure and very good coherence properties. Indeed, on-demand read-out has been demonstrated with bright pulses in a praseodymium-doped crystal [33], and europium adds the potential of larger bandwidth, higher multimode capacity and long storage times [26]. The efficiency is directly linked to the optical depth of the material [26], and can, for example, be addressed by using longer crystals [20]. Alternatively, optical cavities can be used to increase the effective interaction length [34, 35] without material specific side effects. It will be exciting to follow how these developments lead to the actual realisation of a quantum repeater.

We note that, parallel to this work, Saglamyurek *et al.* have also demonstrated storage and retrieval of an entangled photon using a thulium-doped lithium niobate waveguide [36].

Acknowledgements. We thank Reto Locher for help during the early stages of the experiment. We are very grateful to Alexios Beveratos and Wolfgang Tittel for lending us APDs. This work was supported by the Swiss NCCR Quantum Photonics, as well as by the European projects QuRep and ERC-Qore. F.B. was supported in part by le Fonds québécois de la recherche sur la nature et les technologies (FQRNT).

SUPPLEMENTARY INFORMATION

Atomic Frequency Comb

The atomic frequency comb (AFC) memory is a photon-echo based scheme, where the absorption profile of the crystal is shaped into a comb-like structure using optical pumping, thus making it possible to take full advantage of the high atomic density in a doped crystal, despite of inhomogeneous broadening [26].

When a photon enters the crystal, with a spectral bandwidth covering a large part of the AFC spectrum, it is absorbed, provided that the optical depth is sufficient. After the absorption, the photon is stored in a single atomic excitation delocalized over all the atoms, corresponding to a collective Dicke type state,

$$|\Psi(t)\rangle \propto \sum_j^N c_j e^{-ikz_j} e^{i2\pi\delta_j t} |g_1 \cdots e_j \cdots g_N\rangle. \tag{7}$$

In the AFC the distribution of atomic detunings δ_j is periodic with period Δ. After a time $t_s = 1/\Delta$, the components of the state (7) are in phase and lead to the reemission of a photon in a well defined spatial mode $\vec{k}$ with high probability.

Here we used a storage medium composed of $\sim 10^9$ Nd^{3+} dopant ions in an Y_2SiO_5 crystal cooled to 3 K. This crystal has already shown a high multimode capacity [8] with efficiencies between 6% (for $t_s = 100$ ns) and 1% ($t_s = 1.5$ μs). In the work presented here we have improved the storage efficiency in the range $t_s = 25$ to 200 ns by creating comb peaks with an approximate square shape. This has been shown to be the optimal shape in terms of storage efficiency [23]. Note also that the

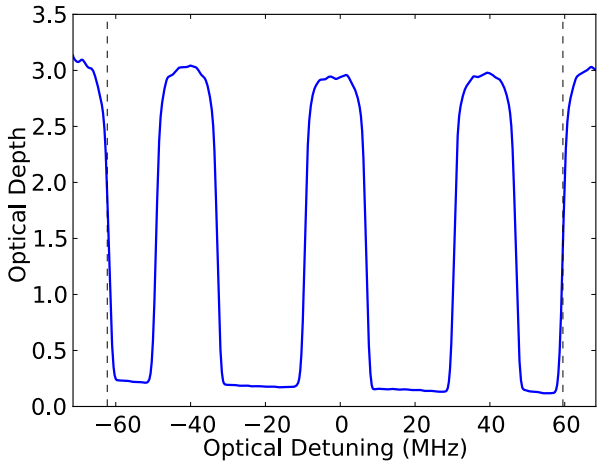

FIG. 4. **Spectrum of an AFC prepared by an incoherent optical pumping technique.** The peaks have a width larger than the effective linewidth of the material, so it is possible to use the whole available optical depth and to have almost square-shaped peaks, which optimizes the rephasing. The dashed lines delimit the 120 MHz bandwidth of the AFC.

AFC structure is prepared by using an incoherent optical pumping technique consisting of simultaneously sweeping the laser frequency and modulating its intensity, as also used in [22]. As a result we observe an efficiency of 21% for $t_s = 25$ ns and 12% for $t_s = 100$ ns. The decay of the efficiency with longer storage time (thus for closer comb spacing Δ) is due to limitations in the coherence properties of the material, which deteriorates the comb shape for closely spaced peaks. We refer to Ref. [8] for a more detailed discussion on this optical pumping issue. For the shortest storage time of 25 ns, however, this problem was almost negligible. Hence, the obtained efficiency is mainly limited by the absorption depth of the crystal. An example of a close to optimal comb for $t_s = 25$ ns is shown in Fig. 4. Using the measured comb as an input to a numerical Maxwell-Bloch simulation gave an efficiency close to the measured one.

Spectral filtering of photon pairs

An overview of the various filtering steps for each of the two wavelengths is given in Table I (see also Fig. 1). As a first filtering step a diffraction grating spatially separates the pump, signal and idler photons and, in combination with coupling into single-mode fibers, it reduces the bandwidth of the photons at 883 (1338) nm to 90 (60) GHz. At 1338 nm, the photons are filtered to their final linewidth of 45 MHz by coupling through a Fabry-Perot cavity with free spectral range (FSR) 23.9 GHz. Additional longitudinal modes of the cavity are subsequently removed by a Fiber Bragg grating with 16 GHz bandwidth.

Filtering one of the photons in the pair is the same as filtering the photon pair as a whole, since energy conservation guarantees that photons measured in coincidence have the same bandwidth. However, uncorrelated photons would then contribute significantly to the accidental coincidences. Therefore, additional filtering at 883 nm was necessary. To this end, we use one solid and one air-spaced etalon, both with bandwidths around 600 MHz. Different FSRs of 42 and 50 GHz eliminate spurious longitudinal modes. Additionally, outside the 120 MHz bandwidth of the AFC the absorption of the crystal with an inhomogeneous linewidth of 6 GHz provides a final filtering step.

We use detectors with 30% detection efficiency and 100 Hz dark counts at 883 nm, and 8% and 10 Hz at 1338 nm. The overall detection efficiencies, which are detailed in Table I, are approximately equal to 0.15% at 1338 nm and 0.5% at 883 nm. This includes losses of the switch and all other optical elements.

Measurements and frequency stabilization

All experiments consisted of a two-part cycle with 15 ms used for the preparation of the AFC and frequency stabilization of the setup, and 15 ms of actual measurement where photons are stored. A fiber optic switch allows for rapid switching between preparation and measurement, and a combination of choppers and acousto-optic modulators efficiently protects the highly sensitive Si APD from the preparation light, which at the position of the crystal has a power of about 1 mW.

The experimentally relevant quantity in all our measurements is coincidence statistics, i.e. the time between the detection of the telecom photon and its partner at 883 nm. Typical rates are a few coincidences per minute. With accumulation times reaching several hours, a high degree of frequency stability of the lasers and filtering elements are indispensible. In particular drifts of the AFC preparation laser with respect to the pump laser of the source had to be eliminated. Otherwise, the photon-pair frequencies $\omega_{883} + \omega_{1338} = \omega_{532}$ imposed by energy conservation in the SPDC would not simultaneously match the center of the AFC and that of the filtering system at 1338 nm. Drifts were eliminated using the following method. First, the long-term stability of the 883 nm laser was dramatically increased by locking it to a temperature stabilized Fabry-Perot cavity. Second, during the 15 ms preparation cycle, we injected a fraction of the 883 nm light into the waveguide. The frequency of the light created at 1338 nm via difference frequency generation (DFG) was then locked to the filtering cavity using a side-of-fringe technique. As a result, long-term frequency deviations between the center of the AFC structure and the filtered photon pairs were reduced to about 1 MHz

TABLE I. **Spectral filtering of photon pairs.** Overview of bandwidth and efficiency for the elements of the optical setup, where the efficiency for optical elements equals the peak transferred intensity normalized to incoming intensity. The free spectral ranges (FSR) of etalons and cavity, as well as the dark count rate (DC) of the detectors, are given in parenthesis.

Wavelength	Element	Bandwidth	Efficiency
883 nm	Grating	90 GHz	70%
	Solid etalon (FSR 42 GHz)	600 MHz	80%
	Air-spaced etalon (FSR 50 GHz)	600 MHz	80%
	AFC	120 MHz	–
	Fiber coupling, polarization controller, fiber optic switch, mirrors, lenses and windows	–	4%
	Detector (DC 100 Hz)	–	30%
	Total	120 MHz	0.5%
1338 nm	Grating	60 GHz	90%
	Filter Cavity (FSR 24 GHz)	45 MHz	30%
	Fiber Bragg Grating	16 GHz	50%
	Fiber coupling, circulator, polarization controller, fiber beam splitter and mirrors	–	14%
	Detector (DC 10 Hz)	–	8%
	Total	45 MHz	0.15%

over several hours.

For measurements involving the unbalanced interferometer for the telecom photon, the phase of the interferometer was also stabilized using the highly coherent DFG light.

CHSH inequality with partial read-outs

We give here some experimental details of the violation of the CHSH inequality [6] using the entangled photon pairs after the signal mode has been stored in and released from the AFC quantum memory.

Our source produces photon pairs entangled in energy and time [5]. Due to post-selection we can simplify the following treatment by considering just two particular temporal modes delayed by τ, the early and late modes

$$\frac{1}{\sqrt{2}}\left(|E_s E_i\rangle + |L_s L_i\rangle\right), \tag{8}$$

where τ is larger than the coherence time of the individual modes. The usual way to highlight time-bin entanglement is to measure two-photon interference in a Franson setup [5] involving two unbalanced interferometers with path length difference τ. By choosing appropriately the measurement settings, i.e. the phases and the beam splitting ratio of the interferometers, the non-local characteristic of this interference can be revealed through the violation of a Bell inequality, e.g. the CHSH inequality. Interestingly, Bell tests can be seen as entanglement witnesses proving that, at any step before the detection, the entanglement produced at the level of the source is preserved, at least partially; see below.

In our setup (see Fig. 1), we use a fiber interferometer for the idler photon. For the signal photon, the interferometer is implemented using partial read-outs of the quantum memory [21].

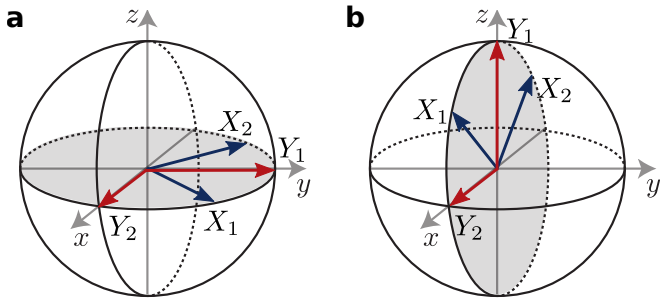

FIG. 5. **Measurement bases for the violation of the CHSH inequality.** Blue (red) arrows indicate signal (idler) bases X_1 and X_2 (Y_1 and Y_2). (a) For the violation of the CHSH inequality, all four bases lie on the equator of the Bloch sphere with the appropriate angles between them. (b) The hybrid qubit represents a state will unequal populations, and optimal violation can only be obtained on a plane including the poles of the Bloch sphere.

The measurement of the CHSH inequality requires two bases for the signal photon X_1 and X_2, and similarly Y_1 and Y_2 for the idler photon. To obtain maximum violation, a possible choice of bases is shown in Fig. 5a. All four bases lie on the equator of the Bloch sphere, X_1 and X_2 form an angle of 90°, and Y_1 and Y_2 are obtained by rotating X_1 and X_2 by 45°. This is the case here, since the probabilities to detect a photon that has taken a long or short path is the same, for both signal and idler; see Fig. 3a. The angles between the bases are given by the relative phases induced by the fiber interferometer and the storage in the AFC. The relative phase in the AFC is controlled by shifting the comb pattern with respect

to the central frequency of the signal photon [26]. In the fiber interferometer, we use the light produced by DFG to set the phase. This light has a coherence time much longer than $\tau = 25$ ns and does show single-photon interference in the interferometer. The interferometer is then stabilized to maintain a certain point on the resulting interference fringe.

Since we had only one detector in each side, we had to add a π-phase shift every time we wanted to access the second outcome of the chosen basis. For this reason, we had to make 4 measurements per correlator, i.e. 16 for the whole Bell test. For a pump power of 3 mW we obtained

$$\begin{aligned} E(X_1Y_1) &= 0.68 \pm 0.12, \\ E(X_2Y_1) &= 0.79 \pm 0.10, \\ E(X_1Y_2) &= 0.60 \pm 0.10, \\ E(X_2Y_2) &= -0.57 \pm 0.14, \end{aligned}$$

leading to $S = 2.64 \pm 0.23$. Here, the uncertainties are standard deviations related to the poissonian statistics of the coincidence events. This is a clear violation of the CHSH inequality and proves not only the conservation of the entanglement during the storage, but that the telecom photon was entangled with a collective excitation in the crystal.

CHSH inequality with a hybrid qubit

The violation of the CHSH inequality using the hybrid qubit is done in analogue to the violation with partial read-outs described above. However, we now want to reveal the entanglement between a photonic time-bin qubit, at telecommunication wavelength, (corresponding to the idler mode) $|E_i\rangle + |L_i\rangle$ and a hybrid light-solid qubit $|E_{QM}\rangle + |L_s\rangle$ that is a superposition between a single-atomic excitation delocalized in a solid and a photonic state (associated to the signal mode).

Instead of using the double read-out to analyze the signal photon, only the early mode $|E_s\rangle$ is stored in the AFC. It is released after a time delay of exactly τ. The detection of this mode, which we will hereafter refer to as *echo*, is thus made indistinguishable from the detection of the late $|L_s\rangle$ mode, which is directly transmitted through the memory. Taking the echo efficiency η_{echo} and the transmission probability η_{trans} into account, this corresponds to a projection onto the vector

$$\cos\theta\langle L_s| + e^{i\phi_s}\sin\theta\langle E_s|, \tag{9}$$

with $\cos\theta = \sqrt{\frac{\eta_{\text{trans}}}{\eta_{\text{trans}}+\eta_{\text{echo}}}}$, and $\sin\theta = \sqrt{\frac{\eta_{\text{echo}}}{\eta_{\text{trans}}+\eta_{\text{echo}}}}$. The phase factor is controlled via the AFC structure [26] and is chosen to be either $\phi_{s,1} = 0°$ or $\phi_{s,2} = 180°$. This corresponds to measuring the following operators with eigenvalues $\{+1, -1\}$,

$$\begin{aligned} X_1 &= \sin 2\theta\ \sigma_x + \cos 2\theta\ \sigma_z, \\ X_2 &= -\sin 2\theta\ \sigma_x + \cos 2\theta\ \sigma_z, \end{aligned}$$

where σ_x and σ_z are Pauli matrices.

Fifty metres away, the idler photon, at telecommunication wavelength, is projected either onto the z-direction (corresponding to the operator $Y_1 = \sigma_z$) by measuring the time of arrival at the detector or onto the x-direction ($Y_2 = \sigma_x$) using a Michelson interferometer. One then finds for the correlators,

$$\begin{aligned} E(X_1Y_1) &= E(X_2Y_1) = \cos(2\theta) \\ E(X_1Y_2) &= -E(X_2Y_2) = \sin(2\theta). \end{aligned}$$

so that the CHSH polynomial $S = 2\cos(2\theta) + 2\sin(2\theta)$ is maximized to $2\sqrt{2}$ for $\cos 2\theta = \frac{\eta_{\text{trans}}-\eta_{\text{echo}}}{\eta_{\text{trans}}+\eta_{\text{echo}}} = \frac{\sqrt{2}}{2}$, i.e. for a ratio between the echo and transmitted pulses

$$\frac{\eta_{\text{echo}}}{\eta_{\text{trans}}} \approx \frac{1}{5.8}, \tag{10}$$

which corresponds to the bases indicated in Fig. 5b. This result is intuitive, as it simply corresponds to the settings of Fig. 5a rotated around the x-axis.

In the experiment, the AFC structure is modified to satisfy this requirement. (We measured $\eta_{\text{trans}} \approx 0.36$, $\eta_{\text{echo}} \approx 0.05$, giving a ratio of 1/7.2). Under the assumption that the marginals are the same for the telecom photon, independent of the result of the measurement on the signal mode, we measure

$$\begin{aligned} E(X_1Y_1) &= 0.68 \pm 0.05 \\ E(X_2Y_1) &= 0.71 \pm 0.06 \\ E(X_1Y_2) &= 0.63 \pm 0.09 \\ E(X_2Y_2) &= -0.60 \pm 0.09 \end{aligned}$$

leading to $S = 2.62 \pm 0.15$, a violation of the CHSH inequality by more than 4 standard deviations. This clearly shows that when the early mode was stored in our solid, the two qubit state involving the hybrid qubit and the telecom qubit was entangled.

Taking a closer look, it might at first be surprising that the violation of the Bell inequality can be maximal, since directly after the absorption the system is described by the *non*-maximally entangled state (neglecting noise)

$$\frac{1}{\sqrt{1+\alpha^2}}\left(\alpha|E_{QM}E_i\rangle + |L_sL_i\rangle\right), \tag{11}$$

where α is related to the absorption efficiency η_{abs} of the quantum memory by $\alpha = \sqrt{\eta_{\text{abs}}}$. (The absorption efficiency corresponds to the absorption by the comb peaks and does not include the absorption by residual atoms whose resonance frequencies fall between the peaks, so that $\eta_{\text{trans}} \neq 1 - \eta_{\text{abs}}$.) The explanation is that the

memory based measurement is a generalized measurement. More precisely, assuming that $\eta_{\rm echo} = \eta_{\rm abs}^2 \eta$ [26], the measurement consists of two generalized measurements $\{X_1', X_2'\}$ made from $\{\Pi_{+1}^s, \Pi_{-1}^s, 1 - \Pi_{+1}^s - \Pi_{-1}^s\}$, i.e. projections onto the non-orthogonal vectors

$$\Pi_{+1}^s : \sqrt{\eta_{\rm trans}}\langle L_s| + e^{i\phi_s}\sqrt{\eta\eta_{\rm abs}}\langle E_{QM}|,$$
$$\Pi_{-1}^s : e^{i(\phi_s+\pi)}\sqrt{\eta}\eta_{\rm abs}\langle L_s| + \sqrt{\frac{\eta_{\rm trans}}{\eta_{\rm abs}}}\langle E_{QM}|,$$

where ϕ_s is controlled from the AFC structure to be either $\phi_{s,1} = 0°$ or $\phi_{s,2} = 180°$ for X_1 and X_2 respectively. Under the fair sampling assumption where inconclusive results are discarded, one can only take successful projections on Π_{+1}^s and Π_{-1}^s into account. If one assigns the value $+1$ (-1) to a conclusive projection into Π_{+1}^s (Π_{-1}^s), one finds random marginals and a Bell violation of $2\sqrt{2}$ provided that the condition (10) is fulfilled. This is analogue to the distillation of entanglement reported in ref. [37] where a non unitary filtering process equalizes the contributions of the two terms in Eq. (11), thereby yielding optimal CHSH violation from a non-maximally entangled state.

---

* These authors contributed equally to this work.

[1] Briegel, H.-J., Dür, W., Cirac, J. I. & Zoller, P. Quantum repeaters: The role of imperfect local operations in quantum communication. *Phys. Rev. Lett.* **81**, 5932–5935 (1998).

[2] Duan, L.-M., Lukin, M. D., Cirac, J. I. & Zoller, P. Long-distance quantum communication with atomic ensembles and linear optics. *Nature* **414**, 413–418 (2001).

[3] Sangouard, N., Simon, C., de Riedmatten, H. & Gisin, N. Quantum repeaters based on atomic ensembles and linear optics (2009). arXiv:0906.2699.

[4] Kimble, H. J. The quantum internet. *Nature* **453**, 1023–1030 (2008).

[5] Franson, J. D. Bell inequality for position and time. *Phys. Rev. Lett.* **62**, 2205–2208 (1989).

[6] Clauser, J. F., Horne, M. A., Shimony, A. & Holt, R. A. Proposed experiment to test local hidden-variable theories. *Phys. Rev. Lett.* **23**, 880–884 (1969).

[7] Simon, C. *et al.* Quantum repeaters with photon pair sources and multimode memories. *Phys. Rev. Lett.* **98**, 190503 (2007).

[8] Usmani, I., Afzelius, M., de Riedmatten, H. & Gisin, N. Mapping multiple photonic qubits into and out of one solid-state atomic ensemble. *Nat Commun* **1**, 1–7 (2010).

[9] Blinov, B. B., Moehring, D., Duan, L.-M. & Monroe, C. Observation of entanglement between a single trapped ion and a single photon. *Nature* **428**, 153–7 (2004).

[10] Volz, J. *et al.* Observation of entanglement of a single photon with a trapped atom. *Phys. Rev. Lett.* **96**, 030404 (2006).

[11] Matsukevich, D. N. & Kuzmich, A. Quantum state transfer between matter and light. *Science* **306**, 663–666 (2004).

[12] Matsukevich, D. N. *et al.* Entanglement of a photon and a collective atomic excitation. *Phys. Rev. Lett.* **95**, 040405 (2005).

[13] de Riedmatten, H. *et al.* Direct measurement of decoherence for entanglement between a photon and stored atomic excitation. *Phys. Rev. Lett.* **97**, 113603 (2006).

[14] Chen, S. *et al.* Demonstration of a stable atom-photon entanglement source for quantum repeaters. *Phys. Rev. Lett.* **99**, 180505–4 (2007).

[15] Sherson, J. F. *et al.* Quantum teleportation between light and matter. *Nature* **443**, 557–560 (2006).

[16] Jin, X.-M. *et al.* Quantum interface between frequency-uncorrelated down-converted entanglement and atomic-ensemble quantum memory (2010). arXiv:1004.4691.

[17] Togan, E. *et al.* Quantum entanglement between an optical photon and a solid-state spin qubit. *Nature* **466**, 730–734 (2010).

[18] Tittel, W. *et al.* Photon-echo quantum memory in solid state systems. *Laser & Photonics Reviews* **4**, 244–267 (2010).

[19] Longdell, J. J., Fraval, E., Sellars, M. J. & Manson, N. B. Stopped light with storage times greater than one second using electromagnetically induced transparency in a solid. *Phys. Rev. Lett.* **95**, 063601 (2005).

[20] Hedges, M. P., Longdell, J. J., Li, Y. & Sellars, M. J. Efficient quantum memory for light. *Nature* **465**, 1052–1056 (2010).

[21] de Riedmatten, H., Afzelius, M., Staudt, M. U., Simon, C. & Gisin, N. A solid-state light-matter interface at the single-photon level. *Nature* **456**, 773–777 (2008).

[22] Lauritzen, B. *et al.* Telecommunication-wavelength solid-state memory at the single photon level. *Phys. Rev. Lett.* **104**, 080502 (2010).

[23] Chanelière, T., Ruggiero, J., Bonarota, M., Afzelius, M. & Gouët, J.-L. L. Efficient light storage in a crystal using an atomic frequency comb. *New Journal of Physics* **12**, 023025 (2010).

[24] Sabooni, M. *et al.* Storage and recall of weak coherent optical pulses with an efficiency of 25%. *Phys. Rev. Lett.* **105**, 060501 (2010).

[25] Akiba, K., Kashiwagi, K., Arikawa, M. & Kozuma, M. Storage and retrieval of nonclassical photon pairs and conditional single photons generated by the parametric down-conversion process. *New Journal of Physics* **11**, 013049 (2009).

[26] Afzelius, M., Simon, C., de Riedmatten, H. & Gisin, N. Multimode quantum memory based on atomic frequency combs. *Phys. Rev. A* **79**, 052329–9 (2009).

[27] Lee, C. T. Nonclassical photon statistics of two-mode squeezed states. *Phys. Rev. A* **42**, 1608–1616 (1990).

[28] Nunn, J. *et al.* Multimode memories in atomic ensembles. *Phys. Rev. Lett.* **101**, 260502 (2008).

[29] Peres, A. Separability criterion for density matrices. *Phys. Rev. Lett.* **77**, 1413–1415 (1996).

[30] Acín, A., Gisin, N. & Masanes, L. From Bell's theorem to secure quantum key distribution. *Phys. Rev. Lett.* **97** (2006).

[31] Bussières, F., Slater, J. A., Jin, J., Godbout, N. & Tittel, W. Testing nonlocality over 12.4 km of underground fiber with universal time-bin qubit analyzers. *Phys. Rev. A* **81**, 052106 (2010).

[32] Sangouard, N. *et al.* Robust and efficient quantum repeaters with atomic ensembles and linear optics. *Phys. Rev. A* **77**, 062301 (2008).

[33] Afzelius, M. *et al.* Demonstration of atomic frequency

comb memory for light with spin-wave storage. *Phys. Rev. Lett.* **104**, 040503 (2010).

[34] Afzelius, M. & Simon, C. Impedance-matched cavity quantum memory. *Phys. Rev. A* **82**, 022310 (2010).

[35] Moiseev, S. A., Andrianov, S. N. & Gubaidullin, F. F. Efficient multimode quantum memory based on photon echo in an optimal QED cavity. *Phys. Rev. A* **82**, 022311 (2010).

[36] Saglamyurek, E. *et al.* Broadband waveguide quantum memory for entangled photons (2010). arXiv:1009.0490.

[37] Kwiat, P. G., Barraza-Lopez, S., Stefanov, A. & Gisin, N. Experimental entanglement distillation and 'hidden' non-locality. *Nature* **409**, 1014–1017 (2001).